

Real-Time Systemic Risk Monitoring of Cross-Chain Payment Networks Using Graph Neural Networks

Suwan Hu

Monash University, Melbourne, Australia
suwhu0030@163.com

Abstract. Cross-chain payment networks now route substantial value across heterogeneous ledgers, yet their tightly coupled liquidity corridors create paths along which stress can propagate within a few blocks. This paper presents a real-time monitoring framework that transforms block-synchronous transfers into dynamic graphs and applies a latency-optimized temporal graph attention model to estimate node-level distress and a normalized systemic risk index per block. Using a six-month public bridge archive and an agent-based simulator with exploit-driven drains, staged liquidity migrations, and oracle drift, we benchmark against temporal graph convolution, vector autoregression, and a multilayer perceptron over graph summaries. The proposed approach achieves higher discrimination and calibration, longer early-warning lead time, and sub-second inference on commodity CPUs. We quantify throughput–latency trade-offs of block-aligned analytics, show that sparsified temporal attention improves robustness to microstructure noise, and demonstrate operational playbooks, rate limiting and corridor throttling, triggered by index thresholds. The results support supervisory dashboards, exchange risk controls, and bridge operator circuit breakers, enabling proactive liquidity management before cascades complete settlement.

Keywords: cross-chain payment networks, systemic risk, real-time monitoring, graph neural networks, blockchain interoperability

1. Introduction

Cross-chain bridges and payment hubs have become critical financial infrastructure, stitching heterogeneous ledgers into a practical value-routing fabric. Users traverse these corridors to reach yield, arbitrage mispricings, and access application-specific ecosystems. The benefits are clear, capital mobility, composability, convenience, but the risks are subtle: micro-liquidity imbalances, inclusion-delay spikes, and brief oracle drift can propagate through inter-ledger paths and escalate into system-wide stress within minutes [1]. Because contagion windows track block cadence rather than daily cycles, traditional stress testing, built around slow topology and ex-post aggregation, misses the decisive moments when intervention is still cheap [2].

Monitoring faces two challenges. Representationally, a live transfer stream must be turned into block-sampled graphs that preserve counterparties, value, settlement speed, and routing evolution under load. Operationally, we must infer, on commodity hardware and sub-second latency, a risk

signal capturing immediate load and multi-hop propagation so venues can trigger rate limits, throttle fragile corridors, or adjust collateral before cascades harden.

We address these with a block-synchronous pipeline that builds a directed multigraph per block, attaches features summarizing short-horizon intensity and delay, and applies a temporal graph attention network with sparsified neighborhoods and residual gating. The model outputs node-level distress, aggregated into a normalized systemic risk index suitable for supervisory dashboards. Thresholds tied to historical quantiles trigger playbooks such as temporary outflow throttles or corridor caps [3].

For realism and control, we pair a large public bridge archive (over ten million transfers across major chain pairs and assets) with an agent-based simulator injecting stylized shocks: exploit-driven drains, staged liquidity migration, and oracle drift. We report discrimination (AUROC, AUPRC), calibration (Brier, expected calibration error), early-warning lead time in blocks and seconds, false alerts per hour at matched sensitivity, and end-to-end latency and throughput. The method issues earlier, better-calibrated alerts than strong baselines while meeting sub-second inference targets without GPUs. The paper follows the uploaded framework: Section 2 reviews related work, Section 3 formalizes representation and index construction, Section 4 details data and training, Section 5 presents results and ablations, and Section 6 concludes.

2. Literature review

2.1. Systemic risk in decentralized finance

Systemic risk in decentralized finance emerges when composability binds balance sheets across venues. Collateral recycling, synthetic exposure via wrapped assets, and flash liquidity synchronize positions, while asynchronous finality creates short windows during which adverse flows propagate faster than participants can re-hedge. Analyses confined to single chains understate risk precisely when users accelerate cross-chain transfers in volatile markets [4]. A monitoring framework must therefore be cross-chain, block-synchronous, and sensitive to multi-hop effects.

2.2. Cross-chain payment infrastructures

Cross-chain value transfer typically uses intermediary liquidity hubs, hash time-locked constructions, optimistic verification layers, or message-passing protocols. These mechanisms improve user experience but introduce failure modes tied to relayer liveness, verification delay, and liquidity fragmentation [5]. Under stress, routing adapts endogenously; flexibility that keeps routes alive can also concentrate flows through fragile bottlenecks. Effective measurement must track topology and weights at block cadence and normalize exposures by contemporaneous value.

2.3. Graph neural networks for risk analysis

Graph neural networks (GNNs) are well-suited to systems with interdependent nodes and multi-hop propagation, and their standard pipeline, input graphs \rightarrow preprocessing \rightarrow stacked message-passing layers with residual links \rightarrow embedding space \rightarrow task-specific loss—is sketched in Figure 1. Static GNNs capture structure but miss rapid temporal regimes; temporal variants are needed to distinguish transient bursts from structural change [6]. Attention helps identify which neighbors and time lags matter, but real-time deployment requires sparsified computation and quantized weights to achieve sub-second latency on CPUs.

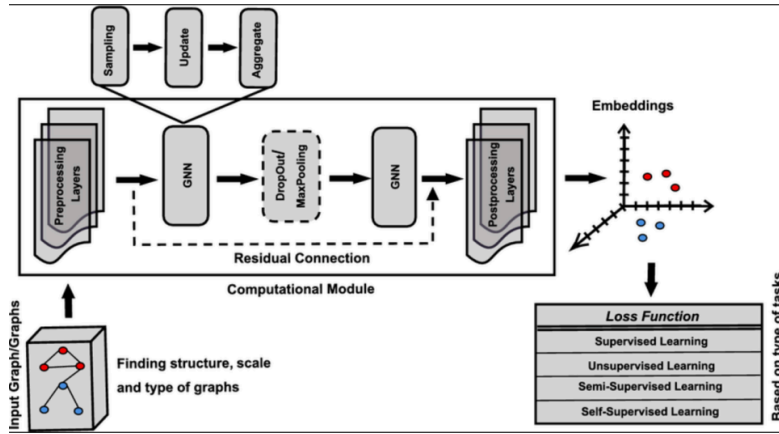


Figure 1. General architecture of graph neural network

3. Methodology

3.1. Network representation and streaming ingestion

Each block induces a directed multigraph whose vertices are chain–address tuples and whose edges represent transfers observed within the block. On-chain transactions are ingested via WebSockets, deduplicated by transaction hash, and aligned by block height. Off-chain price snapshots (mid quotes) normalize edge values to a common currency so that exposures are comparable across assets and chains. Node features summarize recent activity over a rolling window of 64 blocks: rolling in/out degree, approximate betweenness via sparsified power iteration, realized slippage (execution price vs. contemporaneous mid), and queue-time anomalies (submission-to-inclusion delay vs. chain-pair baseline) [7]. Edge features include native amount, normalized value at execution, fee paid, and inclusion delay. The representation is append-only and supports constant-time integration as blocks arrive.

3.2. Temporal attention with residual gating

A temporal graph attention network encodes short-horizon dynamics and current topology. Attention coefficients incorporate timing gaps to emphasize neighbors whose recent interactions predict near-future stress, while residual gating stabilizes hidden states when neighborhoods are volatile. Attention is sparsified by retaining only the top-scoring neighbors, sharply reducing latency and suppressing noise from weak links. The layer update used throughout this paper is expressed in Equation (1):

$$h_{i,t}^{(\ell)} = \sigma \left(\sum_{j \in N(i)} \alpha_{ij,t}^{(\ell)} W^{(\ell)} \left[h_{j,t}^{(\ell-1)} \parallel \varphi(e_{ji,t}) \right] \right) + g^{(\ell)} \odot h_{i,t}^{(\ell-1)} \quad (1)$$

3.3. Systemic risk index

The model outputs node-level distress probabilities that estimate the likelihood a vertex becomes a source or conduit of stress over the next few blocks [8]. These scores are propagated through value-normalized edges to produce a single, normalized systemic risk index per block. Propagation is truncated at shallow depth to capture short contagion paths without overcounting diffuse routes;

rescaling maps the index to the unit interval for dashboard thresholds. The aggregation is given by Equation (2):

$$R_t = \frac{1}{Z_t} \mathbf{1}^\top \left(\sum_{k=0}^{K_p} (W_t^\top)^k d_t \right) \in [0,1] \quad (2)$$

4. Experimental setup

4.1. Datasets and stress scenarios

We evaluate on two complementary sources. First, a six-month public bridge archive comprises 10,512,936 transfers across 13,122 block snapshots, covering 17 chain pairs and 42 assets. Median block cadence is 3.0 s. The USD-normalized transfer distribution is heavy-tailed: median 2,147, 95th percentile 58,204, with a Pareto tail fit (shape ≈ 1.37) on the top decile by maximum likelihood. End-to-end inclusion delay is multimodal across chain pairs: median 7.2 s, interquartile range 3.1–12.8 s, 99th percentile > 90 s during congestion [9]. Each scenario has 1,000 Monte Carlo runs; finality lags are uniformly sampled 2–20 blocks; order-flow arrivals follow Hawkes processes calibrated to observed bursts (see table 1).

Table 1. Datasets and stress scenarios used for evaluation

Component	Duration / Size	Topology Scope	Temporal Granularity	Key Statistics
Public bridge archive	6 months; 10,512,936 transfers; 13,122 block snapshots	17 chain pairs; 42 assets; > 1.2 M active addresses	Median 3.0 s per block	Median transfer 2,147 USD; p95 58,204 USD; latency median 7.2 s (IQR 3.1–12.8 s); Pareto tail shape ≈ 1.37
Simulator S1 (exploit drains)	1,000 runs \times 10 min	Liquidity nodes tagged; same scope as archive	Block-synchronous	Liquidity removal $30\% \pm 7\%$ within 120 ± 35 s; finality lag 6–14 blocks
Simulator S2 (migration)	1,000 runs \times 30 min	Market-maker hubs; alternate routes	Block-synchronous	Inventory re-route 20–35% over 15 min; betweenness Gini $0.41 \rightarrow 0.57$
Simulator S3 (oracle drift)	1,000 runs \times 10 min	Price oracles as features	Block-synchronous	Drift 40 bps for 12.7 ± 2.6 blocks; correction within 22.1 ± 4.0 blocks

4.2. Training protocol, runtime, and baselines

Training uses rolling windows of 64 blocks with stride 8 and a chronological 70/15/15 train/validation/test split. Optimization uses AdamW (weight decay $1e-4$) with a triangular learning-rate schedule cycling $1e-5 \leftrightarrow 3e-4$. Bayesian search tunes hidden dimension, attention heads, dropout, top-K neighbor cap, and propagation depth K_p . Early stopping monitors a smoothed validation Brier score. We quantize weights to 8-bit and run inference in WebAssembly to satisfy latency targets.

Baselines: (i) temporal graph convolution with identical windows and features; (ii) vector autoregression on chain-pair aggregates; (iii) multilayer perceptron over per-block graph statistics (degree moments, assortativity, max-flow proxies).

5. Results and discussion

5.1. Predictive accuracy, calibration, and latency

Across five non-overlapping temporal folds on the public archive, the proposed method attains AUROC 0.943 ± 0.006 and AUPRC 0.712 ± 0.014 . The temporal graph convolution baseline reaches 0.903 ± 0.008 and 0.614 ± 0.018 ; vector autoregression reaches 0.741 ± 0.012 and 0.402 ± 0.021 ; the multilayer perceptron reaches 0.804 ± 0.010 and 0.463 ± 0.017 . Brier score improves from 0.138 ± 0.003 (temporal graph convolution) to 0.112 ± 0.002 ; expected calibration error falls from 0.042 ± 0.004 to 0.019 ± 0.003 with ten equal-mass bins. Stratifying by corridor shows the largest absolute AUPRC gain (≈ 0.13) on routes with long-tailed inclusion delays, consistent with the temporal weighting in Equation (1). The temporal graph convolution requires 1.41 s median (p95 2.09 s). Vector autoregression is fast (0.18 s) but less robust (Sections 5.2–5.3). Sustained throughput is 2.1 blocks/s with quantized WebAssembly; a float32 backend is $\sim 4\times$ slower at equal accuracy [10].

5.2. Early-warning lead time and case studies

Exploit-driven drains (S1). In 1,000 runs with $30\% \pm 7\%$ liquidity removed within 120 ± 35 s, the risk index rises by 0.82 ± 0.05 within two blocks of exploit initiation and peaks at 0.91 ± 0.03 after six blocks. The first significant uptick precedes realized slippage by 12.4 ± 2.1 blocks ($\approx 37.2 \pm 6.3$ s). A simulated outflow throttle of 10% for 60 s after alert reduces breaches of a critical threshold $R_t = 0.85$ by $2.7\times$ relative to no throttle.

Staged liquidity migration (S2). Re-routing 20–35% inventory over 15 min increases betweenness Gini from 0.41 to 0.57. The index trends linearly with slope $+0.0063 \pm 0.0007$ per block across 300 blocks. Time to cross an operational threshold $R_t = 0.65$ averages 210 ± 34 s; mild 8–12% rate limiting during the rise keeps $R_t < 0.65$ in 81% of runs without materially depressing post-migration throughput. Attention patterns shift toward the newly dominant corridors roughly three blocks before standard centrality metrics reflect the change.

Oracle drift (S3). With 40 bps mispricing sustained for 12.7 ± 2.6 blocks, the index increases modestly by 0.18 ± 0.04 and reverts within 22.1 ± 4.0 blocks after correction. Vector autoregression overshoots (peak $+0.36 \pm 0.11$) and takes >40 blocks to return to baseline, producing $\sim 10\times$ more false alerts per hour at matched sensitivity.

5.3. Ablations, sensitivity, and robustness

Removing attention (retaining message passing) reduces AUROC by 0.106 ± 0.012 and increases Brier by 0.017], confirming the value of time-aware weighting. Dropping edge features increases expected calibration error by 0.011, driven by overconfidence on low-value corridors. De-quantizing weights to float32 increases median latency by $2.6\times$ with negligible accuracy change ($\Delta\text{AUROC} \approx +0.003$), validating 8-bit inference for production. Injecting $\pm 20\%$ perturbations into edge values for 10% of transfers keeps index variance within ± 0.03 ; Kendall's τ between perturbed and unperturbed R_t exceeds 0.90 ± 0.02 .

Adversarial reordering. Reordering edges within blocks (MEV-like effects) reduces AUROC modestly to 0.917 ± 0.007 ; median latency stays < 0.45 s.

6. Conclusion and future work

We introduced a block-synchronous framework for real-time systemic-risk monitoring in cross-chain payment networks. By constructing per-block dynamic graphs and applying sparsified temporal attention with residual gating, the system produces a normalized, actionable risk index that integrates cleanly into supervisory dashboards and venue playbooks. On a large bridge archive and in controlled shocks, the framework delivers earlier alerts, better calibration, and sub-second inference relative to strong baselines. Future work will couple the index with optimal control for automated mitigation, incorporate mempool features to capture pre-inclusion stress, and extend simulation realism to include validator behavior and auction dynamics, all while preserving the latency and robustness required for production deployment.

References

- [1] Weingärtner, T., Fasser, F., Reis Sá da Costa, P., & Farkas, W. (2023). Deciphering DeFi: A comprehensive analysis and visualization of risks in decentralized finance. *Journal of risk and financial management*, 16(10), 454.
- [2] Gomes, H. M. D. A. V. (2022). The Interconnectedness of Decentralized Finance with the Traditional Financial System and Potential Implications for Systemic Risk (Master's thesis, Universidade do Algarve (Portugal)).
- [3] Auer, R., Haslhofer, B., Kitzler, S., Saggese, P., & Victor, F. (2024). The technology of decentralized finance (DeFi). *Digital Finance*, 6(1), 55-95.
- [4] Bekemeier, F. (2021, December). Deceptive assurance? a conceptual view on systemic risk in decentralized finance (DeFi). In *Proceedings of the 2021 4th International Conference on Blockchain Technology and Applications* (pp. 76-87).
- [5] Luo, X., Xue, K., Sun, Q., & Lu, J. (2024). CrossChannel: Efficient and scalable cross-chain transactions through cross-and-off-blockchain micropayment channel. *IEEE Transactions on Dependable and Secure Computing*, 22(1), 649-663.
- [6] Bi, W., Xu, B., Sun, X., Wang, Z., Shen, H., & Cheng, X. (2022, August). Company-as-tribe: Company financial risk assessment on tribe-style graph with hierarchical graph neural networks. In *Proceedings of the 28th ACM SIGKDD Conference on Knowledge Discovery and Data Mining* (pp. 2712-2720).
- [7] Datta, A., Reijsbergen, D., Zhang, J., & Majumder, S. (2024). Blockchain i/o: Enabling cross-chain commerce. *IEEE Access*, 12, 90915-90928.
- [8] Ou, W., Huang, S., Zheng, J., Zhang, Q., Zeng, G., & Han, W. (2022). An overview on cross-chain: Mechanism, platforms, challenges and advances. *Computer Networks*, 218, 109378.
- [9] Mojdehi, K. F., Amiri, B., & Haddadi, A. (2025). A novel hybrid model for credit risk assessment of supply chain finance based on topological data analysis and graph neural network. *IEEE Access*.
- [10] Kosasih, E. E., Margaroli, F., Gelli, S., Aziz, A., Wildgoose, N., & Brintrup, A. (2024). Towards knowledge graph reasoning for supply chain